

## Microfluidic Chip Integrated with an Electrolyte-Insulator-Semiconductor Sensor for pH and Glucose Level Measurement

Yen-Heng Lin<sup>1,2,3,\*</sup>, Anirban Das<sup>1</sup>, Min-Hsien Wu<sup>3</sup>, Tung-Ming Pan<sup>1</sup>, and Chao-Sung Lai<sup>1,2,\*</sup>

<sup>1</sup>Department of Electronic Engineering, Chang Gung University, Taoyuan 333, Taiwan

<sup>2</sup>Healthy Aging Research Center, Chang Gung University, Taoyuan 333, Taiwan

<sup>3</sup>Graduate Institute of Medical Mechatronics, Chang Gung University, Taoyuan 333, Taiwan

<sup>4</sup>Graduate Institute of Biochemical and Biomedical Engineering, Chang Gung University, Taoyuan 333, Taiwan

\*E-mail: [yenheng@mail.cgu.edu.tw](mailto:yenheng@mail.cgu.edu.tw); [cslai@mail.cgu.edu.tw](mailto:cslai@mail.cgu.edu.tw)

Received: 30 January 2013 / Accepted: 8 March 2013 / Published: 1 April 2013

---

This paper presents a solid-state sensor, micro-pump, and micro-valve integrated into a microfluidic device that is capable of performing automatic pH level and glucose concentration measurements with small volumes of samples and reagents. Polydimethylsiloxane was used to integrate all of the microfluidic components and was sandwiched between two glass substrate layers with a thin-film metal electrode and reference electrodes. The maximum pumping rate for the pneumatic micro-pump was  $74.6 \mu\text{l min}^{-1}$  at a driving frequency of 25 Hz and an air pressure of 16 psi. Over a time period of 50 s, the washing efficiency achieved was 96%, and a washing buffer did not need to be used when changing between two samples being measured because of the use of a micro-scale channel, which shortened the measurement time. The feasibility of the proposed sensor was demonstrated by measuring pH levels and glucose concentrations. The experimental results showed high sensing linearity (0.9996) for the pH measurement with a sensitivity of  $49.16 \text{ mV pH}^{-1}$ . With the aid of an entrapped-enzyme alginate bead for enzyme delivery and immobilization, glucose concentration was measured with a sensing linearity of 0.9964 and a sensitivity of  $15.05 \text{ mV mM}^{-1}$ , which is higher than using a bulk alginate for enzyme immobilization. In addition, the volume of reagent consumption was greatly reduced to around  $200 \mu\text{l}$ , comparing to the traditional measurement using beaker as a container. With various enzymes encapsulated in the alginate bead, the proposed microfluidic device has the potential to monitor multiple blood indicators at the point of care.

---

**Keywords:** electrolyte-insulator-semiconductor, microfluidics, pH, glucose, solid-state sensor

### 1. INTRODUCTION

Microfluidic systems have a wide variety of applications in biological research. These systems involve the handling of fluids in channels with dimensions of tens to hundreds of micrometers and

have several unique advantages over the traditional approach, including the use of small volumes of samples or reagents, high resolution and sensitivity in separation and detection, short processing times, low cost, and compact size [1]. However, an accurate and easily available sensing technique is crucial for these microfluidic devices. Several sensing techniques that are commonly used for microfluidics include optical, mechanical, magnetic, and electrical approaches. For example, fluorescence analysis is a powerful and sensitive technique for biological sample detection. Laser-induced fluorescence (LIF) detection is the most common method integrated with microfluidic devices for sensitive analysis in the life sciences, such as DNA or immunoglobulin, cells, and microorganisms [2]. SPR devices are capable of performing real-time monitoring of dynamic molecular interactions and analysis of the analytes. A microfluidic chip integrated with an arrayed immunoassay using SPR phase imaging for a specific immunoglobulin has been demonstrated in previous studies [3]. However, such techniques require the use of laser, high-precision mechanical stage, and high-sensitivity optical sensors such as photomultiplier tubes (PMTs), which are too expensive for general use. An alternative to optical methods, based on mechanical stresses produced in a cantilever, has also been adopted for biosensing. Changes on the surface of microfabricated cantilever beams due to mechanical stress bends have been used to sense pH and temperature changes, the formation of self-assembled monolayers, DNA hybridization, antibody–antigen interactions, and the adsorption of bacteria [4]. Magnetoresistance technology has also been used in biological sensors. A force related to the DNA–DNA, antibody–antigen, or ligand–receptor pairs can be measured using this technique. With multiple magnetic transducers fabricated on a chip, thousands of analytes can be measured on a single chip [5]. However, the complexity involved in performing the surface functionalization process on cantilever or magnetic bead and fabricating the sensing chip again prevent the wide use of these devices for biological sample detection. Thus, an easily fabricated, low cost, and high sensitivity sensor is crucial for integration into a microfluidic chip.

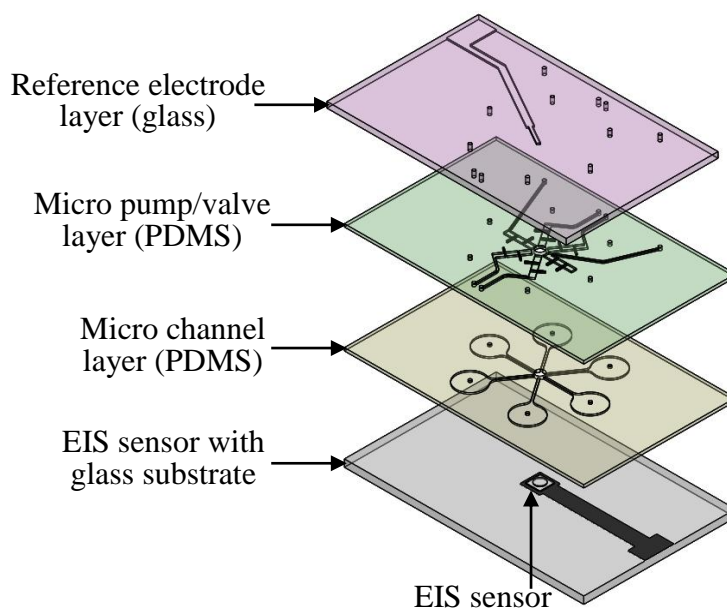
Biosensing techniques using electrical signals have been widely adopted in recent years. For example, the integration of an electrochemical biosensor and microfluidic chip has been demonstrated [6-8]. Multiple targets, such as glucose, lactate, glutamic oxaloacetic transaminase (GOT), glutamic pyruvic transaminase (GPT), pH, ammonia, urea, and creatinine, can be detected in the device. The electrical impedance method can also be integrated in a microfluidic chip, particularly for investigating cells. The measurement of volume changes in a single cell stimulated by a hypotonic solution can be achieved in real time [9]. A solid-state sensor is another type of electric biosensor with a potentiometric property that can transduce a biological reaction into an electrical signal. It was first proposed as a miniaturized, silicon-based chemical sensor by Bergveld (1970) [10]. Because silicon-based devices are currently the basic structural element in the electronics industry, they can be mass produced at a low cost/unit and may be a promising sensing technique for integration into a microfluidic device. The solid-state sensor has several advantages, such as its small size, fast response, high reliability, low output impedance, and ease of integration with a miniaturized system. In addition, by conjugating different types of biorecognition materials on the sensor surface of a solid-state sensor, the sensor can be used for various biological analyses and is referred to as a “BioFET.” The detection of enzymes, proteins, bacteria, cells, and DNA has been demonstrated using this sensing technique [11].

Because the electrical sensing signal transduced by solid-state sensor is easily detected using standard instrumentation, the reading instrument for microfluidic chip incorporating with such type of sensor is ease of commercialization. Furthermore, the fabrication of such sensors is easily achieved using established semiconducting techniques, and thus the unit cost is relatively low. In addition, multiple-sample detection and single-cell investigation should rely on a combination of microfluidics techniques [12-13]. Thus, integrated solid-state sensor and microfluidic devices are regarded as a promising low-cost solution for biological sensing applications. In this study, we investigate the fabrication process of integration of a microfluidic chip with a solid-state EIS sensor, pneumatic micro-pump, and micro-valve for the automatic measurement of sample solution. The pH level and glucose concentration are used to demonstrate the feasibility of the proposed chip. In addition, the performance of the micro-pump and micro-valve were characterized for the handling of liquids. The proposed chip provides rapid detection, low-volume consumption, and automatic control for the detection of sample solution. With the alginate micro-bead enzyme immobilization method, glucose concentrations can be automatically measured in the proposed microfluidic chip.

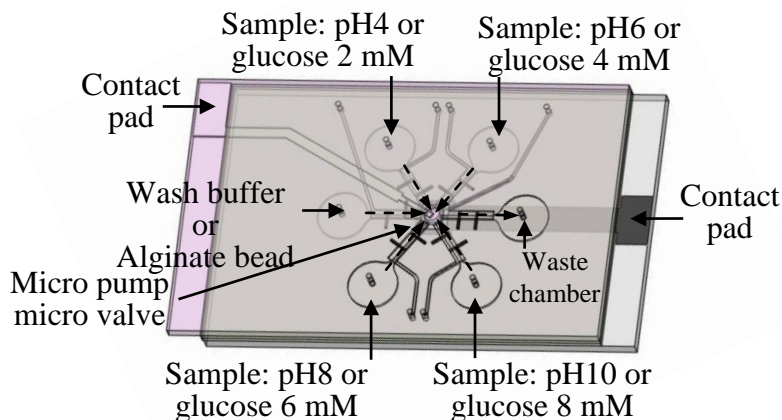
## 2. MATERIALS AND METHODS

### 2.1 Chip design

Figure 1(a) provides an exploded view of the integrated microfluidic chip, which is composed of an EIS solid-state sensor, micro-pumps, and micro-valves. On the bottom of the chip, an EIS sensor is attached to a glass substrate with an aluminum electrode to conduct the sensing signal from the bottom of the EIS sensor.



A



B

**Figure 1.** (a) Exploded view of the proposed microfluidic chip. The micro-pump, micro-valve, and micro-channel are fabricated using PDMS and sandwiched between two glass substrate layers. The top substrate layer is equipped with a thin-film reference electrode and drilled holes. The bottom layer is incorporated with an EIS solid-state sensor for pH level and glucose sensing. (b) The chip equipped with six reservoirs: four for sample loading and one each for a wash buffer and waste chamber. All of the liquid handling could be performed with the aid of the integrated microfluidic components.

Two polydimethylsiloxane (PDMS) layers in the middle of the chip are used to perform the fluid handling function. Six micro-pumps and valves are designed to automatically handle the fluid. Note that the pneumatic micro-pump also serves as a micro-valve. When the fluid has to be transported, the compressed air is alternately switched on and off to drive a PDMS membrane beneath the air chamber, and thus, the fluid is compressed and transported in the micro-channel (see detail in section 2.2). When the compressed air is introduced and held for a period of time, the deflection of the PDMS membrane beneath the air chamber can block the fluid and serve as a valve. The height of the micro-channels is 150  $\mu\text{m}$  except for the channel connected to the wash buffer chamber (200  $\mu\text{m}$ ). The reduction in the micro-channel height from 200  $\mu\text{m}$  to 150  $\mu\text{m}$  provides a barrier to block the enzyme-containing alginate micro-bead for the glucose level measurement (details are provided in section 2.2). On the top of the chip, an Ag/AgCl thin-film reference electrode was fabricated on the glass substrate to provide a reference potential when the measurement is taken.

The chip contains six reservoirs for the preloading of the samples and the wash buffer. The experimental procedure for pH level measurements is described as follows. First, four samples with different pH levels are loaded into the four reservoirs, and the wash buffer is loaded into another reservoir, as shown in fig. 1(b). In the center of the chip, the space that contains the EIS sensor is the reaction chamber. The dotted line drawn in fig. 1(b) shows the direction of the flow. When taking a measurement, a sample with pH 4 in the top left reservoir is first introduced into the reaction chamber with the driving force provided by two pneumatically-driven micro-pumps fabricated on the corresponding sample channel and waste chamber channel. The force generated from the micro-pump

on the waste chamber channel provides a suction force, whereas the micro-pump located on the sample channel provides a pushing force on the fluid. After the sample fills the reaction chamber, all of the micro-valves are closed, and the electric signal is transduced by the EIS sensor and measured by an LCR meter. Having detected the first sample, the second sample with pH 6 is injected into the reaction chamber using the same control method for 3 min. The process is then repeated to detect the third and fourth samples in order. In addition, for a glucose level measurement, an enzyme must be immobilized on the EIS sensor so that the interaction between the glucose sample and enzyme can release hydrogen ions and thus change the potential on the EIS sensor surface. Thus, before the glucose sample is injected, an enzyme-encapsulated alginate micro-bead with an average size of 170  $\mu\text{m}$  is loaded from the wash buffer inlet to carry and trap the enzyme on the sensing surface in the reaction chamber. The reduction in the channel height from 200  $\mu\text{m}$  to 150  $\mu\text{m}$  provides a barrier to the channel entrance to block the enzyme-containing alginate microbead.

## 2.2 Operating principle and sensing theory

The fluid was controlled by pneumatic micro-pump and micro-valve. The detail operating principle of micro-pump is described in supplemental fig. S1. The compressed air is injected repeatedly, causing the micro-pump to generate peristaltic action in a specific direction. Similarly, when the compressed air is applied and held for a period of time, the fluid beneath the PDMS membrane is blocked and prevented from passing through the micro-valve. The micro-pump and micro-valve are realized in the same pneumatic micro-structure.

The change in the flat band voltage ( $V_{FB}$ ) of the EIS sensor can be measured when the surface potential of the sensor is influenced by the surrounding medium. The flat band voltage can be defined in terms of the following equation [14-15]:

$$V_{FB} = E_{ref} - \psi + \chi_{sol} - \frac{\Phi_{si}}{q} - \frac{Q_{SS} + Q_{OX}}{C_{OX}} \quad (1)$$

where  $E_{ref}$  is the reference electrode potential,  $\chi_{sol}$  is the surface dipole potential of the solution,  $\Phi_{si}$  is the silicon work function,  $q$  is the elementary charge,  $Q_{SS}$  is the surface state density per unit area at the silicon surface,  $Q_{OX}$  is the fixed oxide charge per unit area,  $C_{OX}$  is the gate insulator capacitance per unit area, and  $\psi$  is the surface potential. All of the terms in this equation are constant except  $\psi$ , so the flat band voltage is influenced by the surface potential. In addition to the influence of the surrounding medium, the change of the surface potential can also be affected by the reaction between the sample and enzyme that occurs on the sensor surface. Figure 2(a) illustrates the sensing principle for glucose level in the proposed chip. The enzyme-containing alginate microbead is used to deliver and immobilize the enzyme on the sensor surface, after which the glucose molecule reacts with the enzyme in the alginate bead. During the reaction process, the hydrogen ions are released, and the change in the potential on the sensor surface can be transduced by the EIS sensor and detected by the LCR meter. Figure 2(b) shows a schematic of the enzyme-entrapped alginate micro bead. The glucose

oxidase and magnetic powder are encapsulated by the alginate microbead, which is generated by another microfluidic-based pneumatically driven micro-vibrator [16] with an emulsion technique based on our previous study.

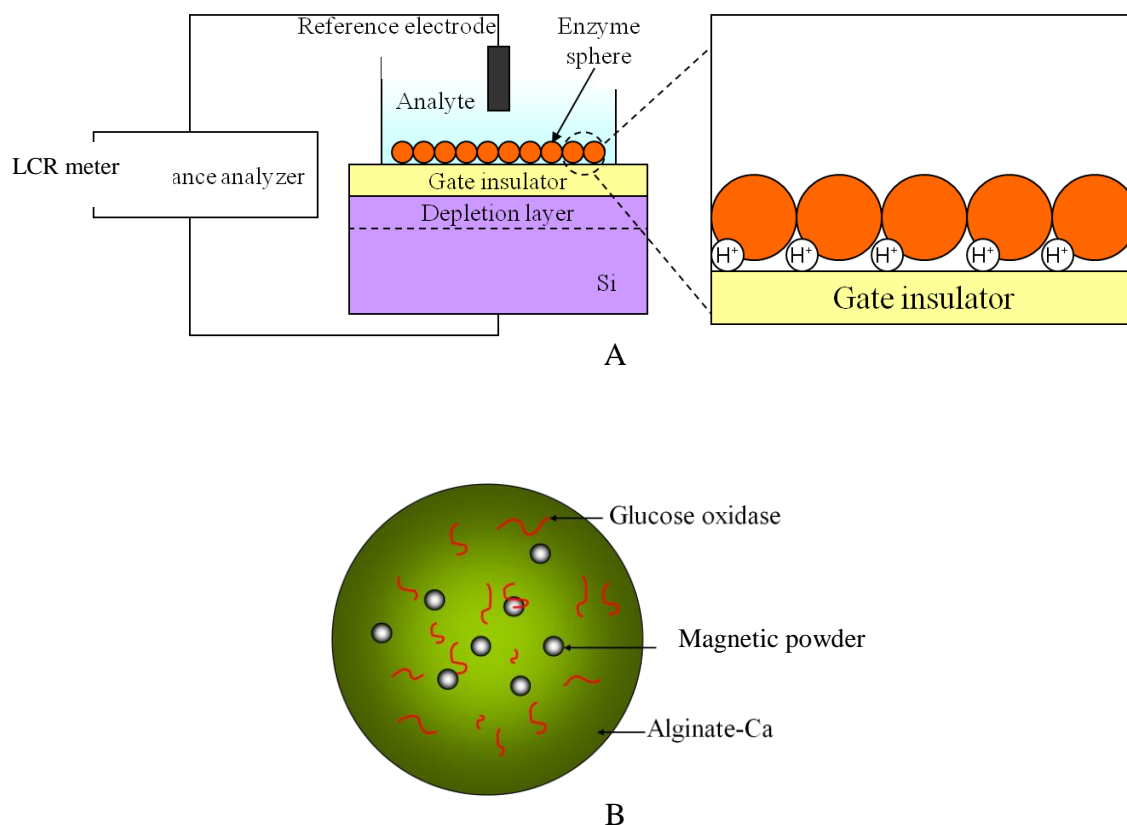


**Figure 2.** (a) Mechanism of sensing glucose in the EIS sensor. First, the enzyme containing the alginate micro-sphere is immobilized on the surface of the EIS sensor. Then, the glucose specimen can react with the enzyme and release hydrogen ions, which change the surface potential of the sensor and can be detected by the impedance analyzer. (b) The schematic illustration of the enzyme-trapped alginate micro-sphere generated by an emulsion technique.

The magnetic powder is used to provide a magnetic force for increasing the packing density of the beads on the sensor surface, thereby increasing the change in the potential.

### 2.3 Chip fabrication and experimental setup

The proposed chip was fabricated through MEMS techniques and the detail fabrication process is described in supplemental fig. S2. The EIS sensor having a 20 nm, high-k,  $Dy_2TiO_5$ -sensing membrane was integrated in microfluidic chip, which was based on our previous work [17]. Note that when the sensor was attached to the glass substrate, a prominent bump-like structure was formed, which may cause a dead volume or instable flow on the sensing region. A thin PDMS layer was used to fill up the bump-like structure and resulted in the same level of sensor surface and PDMS surface (see detail in supplemental fig. S3). During fabrication process, another glass plate was placed on top of the sensor die such that the flat PDMS surface can be formed. A photograph of the assembled chip

is shown in fig. 3; the chip is 8 cm wide and 5 cm long. Because of the naturally hydrophobic property of the PDMS, a surface treatment process was necessary to produce the hydrophilic channel wall so that the fluid could be transported in the chip.

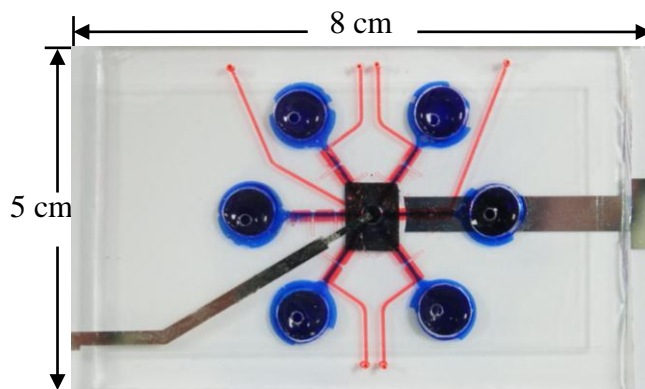


**Figure 3.** Photograph of the assembled microfluidic chip with the dimensions of 8 cm × 5 cm.

A solution of triblock copolymer surfactant (Pluronic P123, MW 5750) was used to modify the PDMS surface such that it exhibited the hydrophilic property. The 2.5% (w/v) P123 solution in 99 wt.% aqueous ethanol was injected into the microfluidic chip and left overnight at room temperature. Then, the unbound P123 was washed away with deionized (DI) water, and the hydrophilic PDMS micro-channel was ready for use.

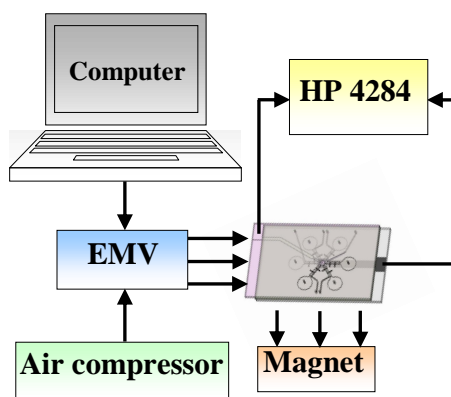


**Figure 4.** Experimental setup for the microfluidic chip. The microfluidic components are controlled with electro-magnetic-valve connected to the compressed air. The electric signal is measured by an LCR meter.

Figure 4 illustrates the experimental set-up for the chip. The pneumatic micro-pump and micro-valve were controlled by an electromagnetic valve (EMV, SMC Inc., S070 M-5BG-32, Taiwan) connected to a compressed air source (JUN-AIR Inc., MDR2-1A/11, Japan) and personal computer. A magnet was used to facilitate the immobilization of the enzyme-containing alginate bead. The electric signals were measured using a Hewlett-Packard 4284A LCR meter operated at an AC signal frequency

of 100 Hz. The measurements were taken in a dark environment to avoid light interference.

All of the chemical reagents were purchased from Sigma-Aldrich, Taiwan. The standard pH solutions were prepared by titrating NaOH and HNO<sub>3</sub> to obtain pH levels of 4.03, 6.70, 7.40, and 9.57. The stock glucose concentration, 8 mM, was then series diluted to obtain concentrations of 6, 4, and 2 mM, which cover the glucose range in human blood. The enzyme-containing alginate microbeads were produced through the emulsion technique described in our previous study [16]. A mixture of 10 mg of glucose oxidase and 2 mg of alginate-Na were dissolved in 100  $\mu$ l DI water and then mixed with another 100  $\mu$ l of magnetic powder dispersed in DI water with a concentration of  $2 \times 10^9$  beads ml<sup>-1</sup>. The alginate-Na droplets were generated and then solidified using 0.4 mM CaCl<sub>2</sub>. The magnetic powder is “Dynabeads” with a diameter of 1  $\mu$ m and no surface functionality (purchased from Invitrogen).

### 3. RESULTS AND DISCUSSION

#### 3.1 Characterization of the pneumatic micro-pump and the washing process

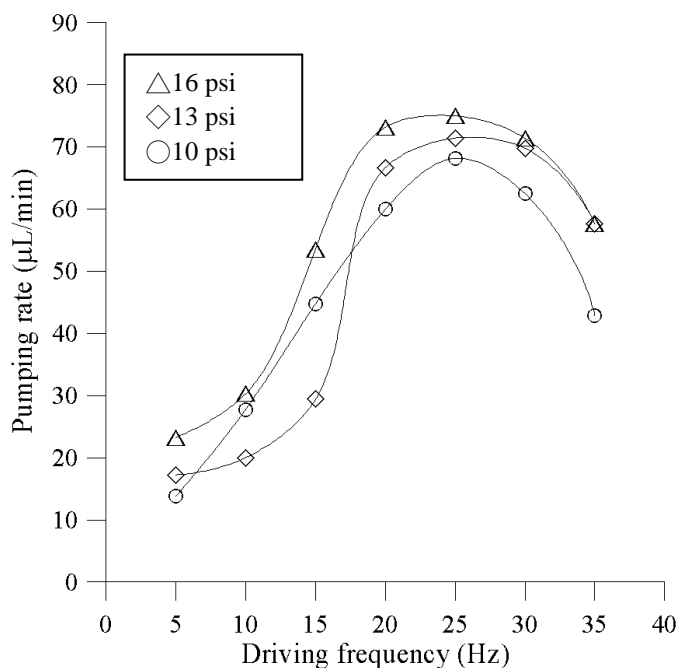
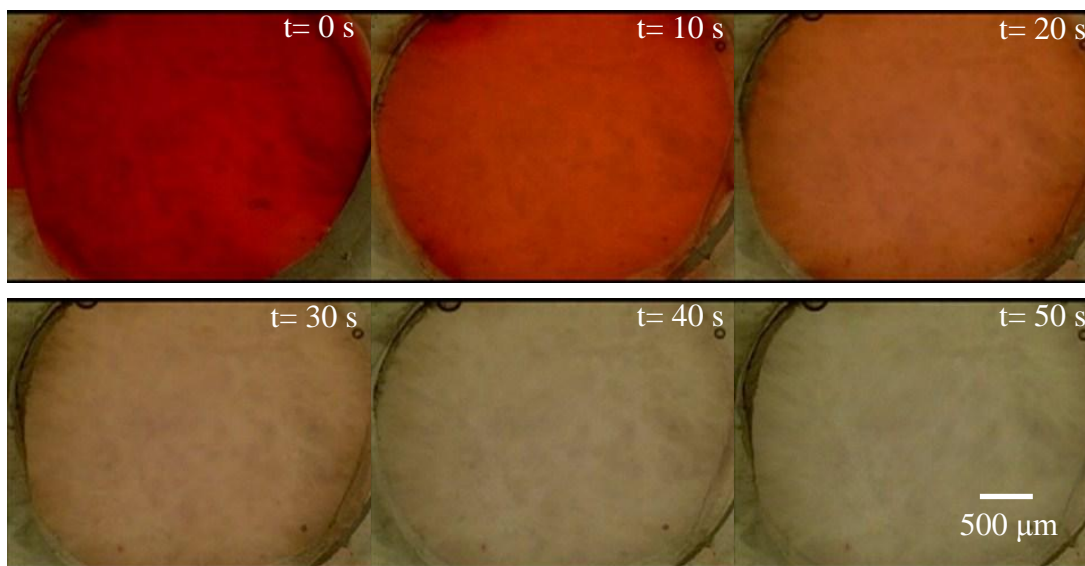


**Figure 5.** Characterization of the micro-pump with the different applied air pressures and driving frequencies to the flow rate. The flow rate increases when the driving frequency is increased (at a constant applied pressure). The maximal flow rate can be generated at a driving frequency of 25 Hz. When the driving frequency is beyond the maximal frequency, the flow rate drops because the air chamber cannot be completely filled and released at such a high frequency.

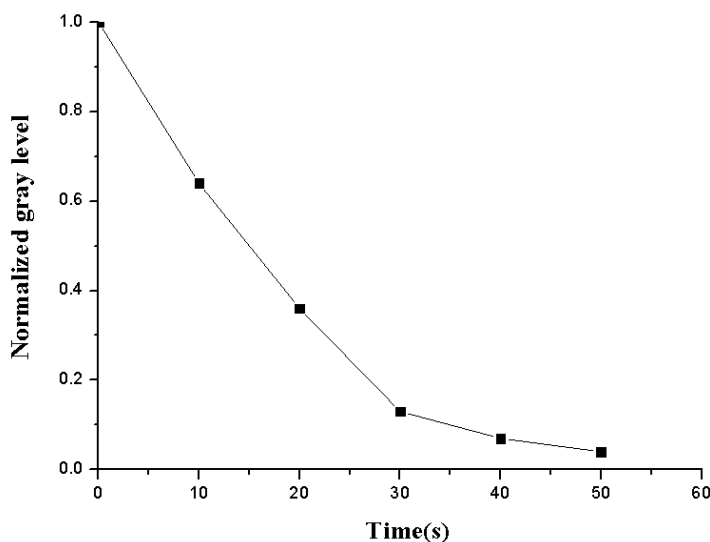
In this study, six pneumatic micro-pumps were integrated in the chip to transport the reagents in the micro-channels. The driving frequency of the micro-pump is controlled by the EMV. The effect of the applied air pressure on the flow rate at different driving EMV frequencies was investigated. Figure 5 reveals the relationship between the pumping rate and driving frequency of the micro-pump at different applied air pressures. The maximum pumping rate of  $74.6 \mu\text{L min}^{-1}$  was obtained at a driving



frequency of 25 Hz and an air pressure of 16 psi. In general, the pumping rate increases with increased frequency until it reaches the maximum because the response time of the pneumatic micro-pump is limited by the fill and release times of the compressed air. When the frequency of the applied air is higher than the response time of the micro-pump, the PDMS membrane beneath the air chamber cannot be deflected completely; thus, the flow rate decreases.



A



B

**Figure 6.** Characterization of the washing process. (a) Photographs of the washing process simulated with red ink over a time period of 50 s. (b) The normalized gray level versus washing time. It can be observed that the sample can be washed 96% within the time period of 50 s at a driving frequency of 25 Hz and an applied air pressure of 16 psi.

For the automatic measurement of samples, a washing process or sample substitution process is performed in the chip. Figure 6(a) shows a series of photographs of the washing process, which was

simulated by red dye washed by DI water within 50 s. The red ink was first transported from the top left reservoir by the two micro-pumps described in section 2.1, and then the continuous air pressure was applied to block the flow. Then, the DI water was introduced from the top right reservoir to wash the red ink. All of the procedures are programmed in custom software with the EMV-aided control. The washing or substitution efficiency achieved was 96% with a time period of 50 s (see fig. 6(b)) and 100% with a time period more than 120 s, which was analyzed using image-processing methods (ImageJ). As a result, the time period of the washing process in all measurements was set to 3 min to ensure a complete substitution of the reagents. Compared to other literatures regarding the combination of solid-state sensor and microfluidics, the integration of micro-pump and micro-valve in this study provides the automatic fluid control and facilitates the convenience for reagent substitution [18-20].

### 3.2 Automatic measurement of four pH levels

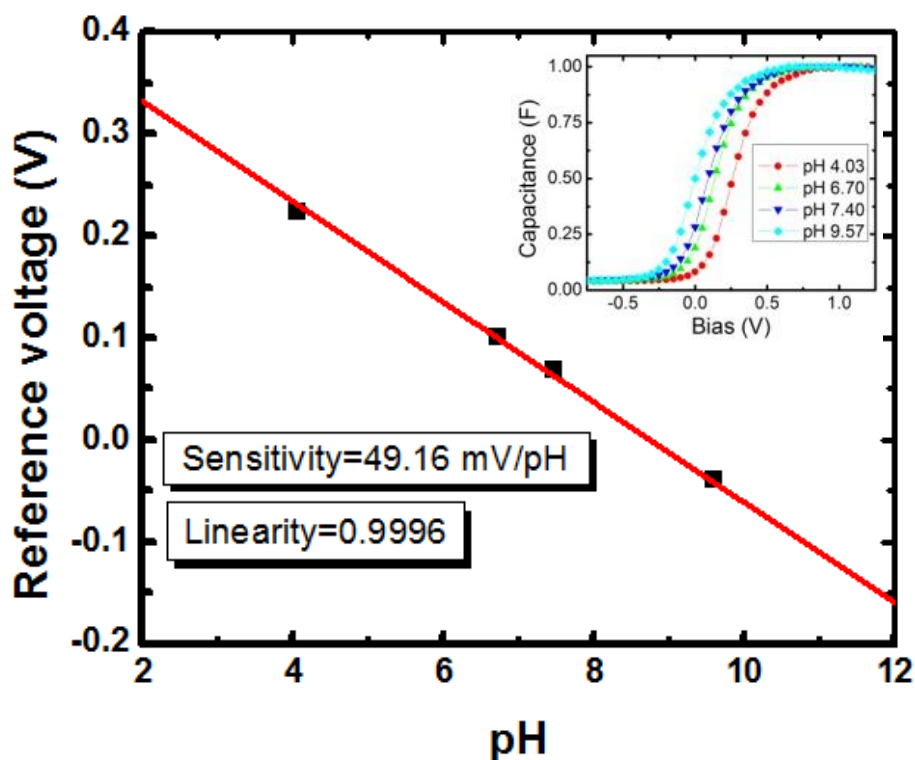


**Figure 7.** The measurement results of pH levels from 4.03 to 9.57. The different pH level solutions were introduced sequentially into the proposed chip, and the corresponding reference voltages were measured accordingly. The sensing linearity was calculated to be 0.9996 with a sensitivity of  $49.16 \text{ mV pH}^{-1}$ . The insert figure shows that the pH dependence of the C-V curves shifted as a result of the change in the number of hydrogen ions on the EIS sensor surface.

Four pH solutions with pH levels of 4.03, 6.70, 7.40, and 9.57 were used to verify the performance of the developed chip. They were loaded into the four reservoirs and then pumped sequentially into the reaction chamber for measurement by the EIS sensor. After the first solution was detected, the second solution was directly introduced for 3 min to replace the previous solution without the use of any wash buffer between the two samples. The process was then repeated to detect the third

and fourth samples. Figure 7 illustrates the measured voltage for the different solutions (pH levels). The results show high sensing linearity (0.9996) for the pH measurement, and the sensitivity was calculated to be  $49.16 \text{ mV pH}^{-1}$ . With high linearity, it can be inferred that the washing process was complete, so the contamination caused by the previous pH level was very low. Because of the small volume and laminar flow property in the micro-scale channel, we determined experimentally that the washing process is not necessary for the sample change. The insert figure depicts the pH dependence of the C-V curves for the EIS sensor. These C-V curves were shifted as a result of the change in the number of hydrogen ions on the EIS sensor surface. The advantage of using microfluidic techniques is that the reagent consumption is greatly reduced comparing to the traditional bulky measurement method. For each pH sample, the volume of consumption was about  $200 \mu\text{l}$ . The other important improvement is that the entire measurement process is done automatically, indicating that it can avoid the contamination caused by manual measurement. In addition, the planar reference electrode in the proposed chip facilitates the miniaturization of the entire microfluidic device, compared to other method with inserting silver wire as a reference electrode [20-21].

### 3.3 Measuring glucose concentration in the chip

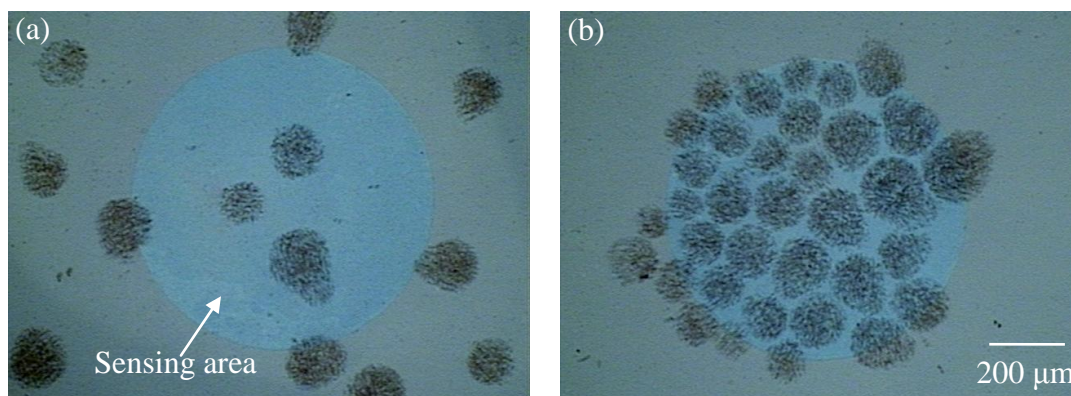


**Figure 8.** Immobilization of the enzyme- and magnetic-bead-contained alginate micro-sphere on the surface of the sensing area. (a) After the alginate micro-sphere was blocked and resuspended in the sensing chamber, the location of the micro-sphere revealed a random distribution on the sensor surface. (b) The magnetic-bead- and enzyme-encapsulated alginate micro-sphere could be further concentrated on the sensing area through an external magnetic force.

For glucose level measurements, the corresponding enzyme must be on the sensor surface. In this study, the supplied enzyme for reacting with the detection sample in the microfluidic chip was carried and immobilized using an alginate micro-bead containing the enzyme and magnetic powders. The alginate micro-beads were generated with a microfluidic emulsion technique using pneumatically driven vibrators [16]. At the appropriate operating condition, with a driving frequency of 2 Hz and a flow rate of  $2 \mu\text{l min}^{-1}$ , an alginate micro-bead with an average diameter of  $170 \mu\text{m}$  was produced. Note that the bead size should be smaller than the inlet channel height and larger than the height of the other five channels, i.e., smaller than  $200 \mu\text{m}$  and larger than  $150 \mu\text{m}$ , so that the bead can be restricted to the reaction chamber by the barrier created by the reduction in the channel height. When the alginate

bead was loaded from the wash buffer inlet with an external vacuum force applied from the waste chamber, approximately 80% of the alginate beads were blocked in the reaction chamber, and the other 20% entered the waste chamber because of the size distribution of the beads. The trapped beads were then re-suspended by the phosphate buffered saline (PBS) buffer in the reaction chamber and revealed a random distribution on the sensor surface (see the detail in fig. 8(a)). With the aid of the external magnetic force, the magnetic powder containing alginate beads was re-arranged inside the 2 mm sensing area of the EIS sensor, as shown in fig. 8(b). In this manner, the change in the potential on the sensor surface could be increased, and the sensitivity of the measurements improved accordingly.

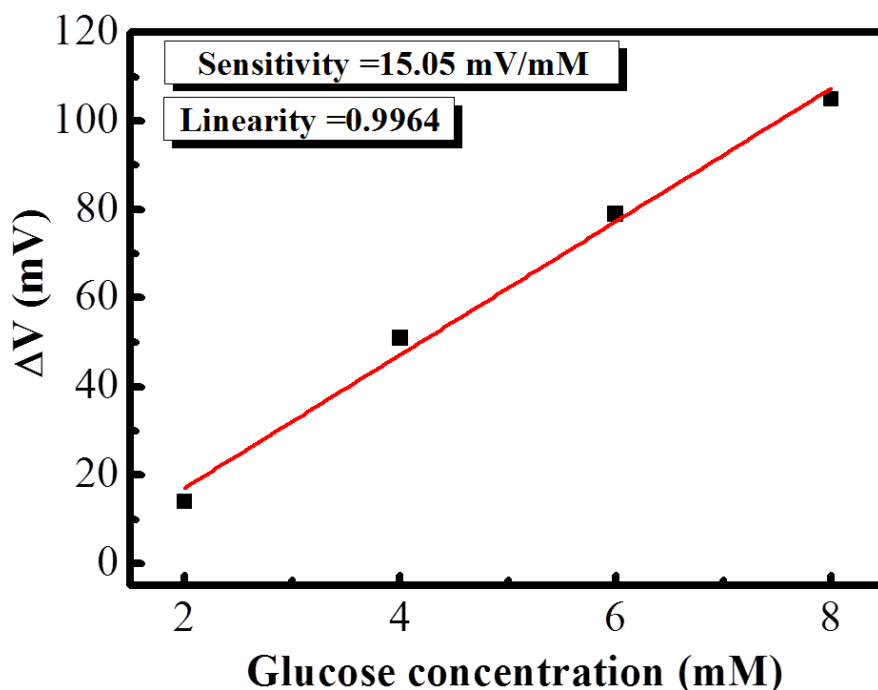


**Figure 9.** The results of glucose concentration measurement in the chip with the aid of the enzyme-encapsulated alginate micro-sphere. The chip revealed high sensing linearity (0.9964), with a sensitivity of  $15.05 \text{ mV mM}^{-1}$ .

After the enzyme-entrapped alginate bead was immobilized in the reaction chamber, four glucose solutions with concentrations of 2, 4, 6, and 8 mM and volume of  $200 \mu\text{l}$  were introduced into the reaction chamber sequentially. Figure 9 shows the measurement results of the glucose levels in the chip. It can be observed that a high sensing linearity of 0.9964 was achieved with a sensitivity of  $15.05 \text{ mV mM}^{-1}$ . Note that as in the pH level measurement, no washing process was required when the new sample was substituted for the old sample. Because of the reduction in the length of mass diffusion, the sensitivity of the glucose measurement is higher using alginate micro-beads than in our previous study, in which a bulk alginate was used for enzyme immobilization and a similar high- $k$  material was used for the sensing membrane ( $7.94 \text{ mV mM}^{-1}$ ) [22]. The use of alginate micro-bead as a carrier provides a simple method for substitution recognition substance on the sensor surface, which is more convenient than other permanent immobilization method for recognition substance such as covalent binding or

cross-linking [23]. In addition, with the encapsulation of other types of enzymes in the alginate bead, the proposed chip has the ability to measure various targets through the same procedure.

#### 4. CONCLUSION

We have demonstrated a microfluidic chip integrated with a solid-state EIS sensor, active micro-pumps, and micro-valves that is capable of measuring pH and glucose levels through automatic fluid control. The reagent consumption is greatly reduced using the proposed chip (approximate 200  $\mu$ l for each sample) comparing to the measurement using beaker as container (approximate 20 ml for each sample). In addition, the automatic-control measurement process can avoid the contamination arose by manual operation. A pneumatic air chamber and PDMS membrane were used to provide the pump and valve functions to achieve the fluid control. When the washing period is set to 3 min, no wash buffer is required for the sample change process, which reduces the volume of reagent and the measurement time. Experimental data show that the measurements of both pH and glucose levels have high linearity in the proposed chip. With enzyme-encapsulated alginate micro-beads, the measurement sensitivity is higher than that of the traditional bulk alginate encapsulation method. Magnetic powder is contained in the alginate bead, so the bead can be further packed and immobilized at the sensing window of the EIS sensor. Otherwise, by changing the entrapped enzyme in the alginate bead, multiple types of samples can be measured using the same chip. The proposed microfluidic device is promising for point-of-care assays.

#### ACKNOWLEDGEMENTS

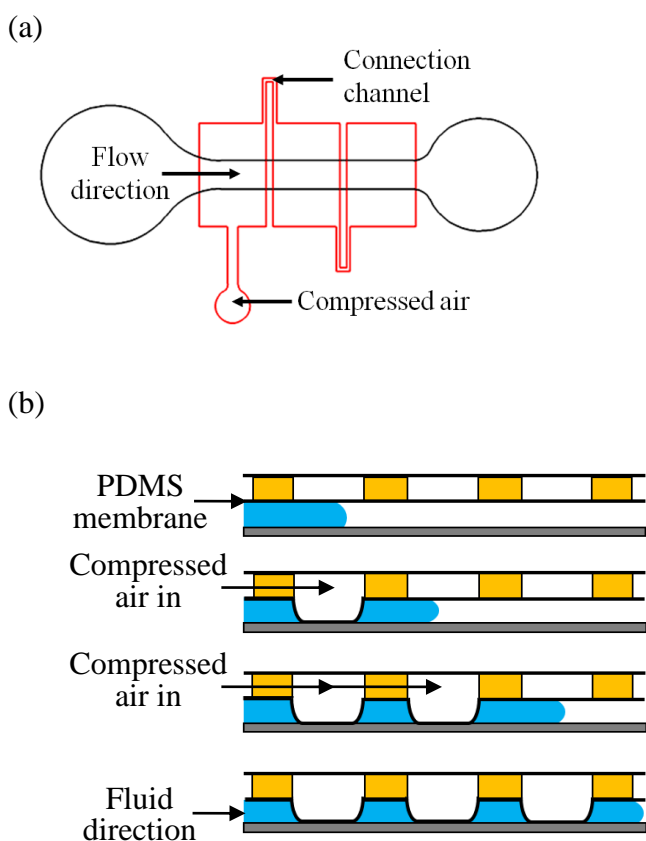
The authors would like to thank the National Science Council of Taiwan for the financial support provided for this study under Grant No. NSC 100-2221-E-182-021-MY3.

#### References

1. G.M. Whitesides, *Nature*, 442 (2006) 368
2. C. Wang, J. Ouyang, D.-K. Ye, J.-J. Xu, H.-Y. Chen and X.-H. Xia, *Lab Chip*, 12 (2012) 2664
3. K.-H. Lee, Y.-D. Su, S.-J. Chen, F.-G. Tseng and G.-B. Lee, *Biosens. Bioelectron.*, 23 (2007) 466
4. J. Fritz, *Analyst*, 133 (2008) 855
5. D.R. Baselt, G.U. Lee, M. Natesan, S.W. Metzger, P.E. Sheehan and R.J. Colton, *Biosens. Bioelectron.*, 13 (1998) 731
6. W. Satoh, H. Hosono, H. Yokomaku, K. Morimoto, S. Upadhyay and H. Suzuki, *Sensors*, 8 (2008) 1111
7. S. Hideshima, R. Sato, S. Kuroiwa and T. Osaka, *Biosens. Bioelectron.*, 26 (2011) 2419
8. Z.E. Selvanayagam, P. Neuzil, P. Gopalakrishnakone, U. Sridhar, M. Singh and L.C. Ho, *Biosens. Bioelectron.*, 17 (2002) 821
9. S.Z. Hua and T. Pennell, *Lab Chip*, 9 (2009) 251
10. P. Bergveld, *IEEE Trans. Biomed. Eng.*, BME-17 (1970) 70
11. M.J. Schöning and A. Poghosian, *Analyst*, 127 (2002) 1137
12. G. Xu, X. Ye, L. Qin, Y. Xu, Y. Li, R. Li and P. Wang, *Biosens. Bioelectron.*, 20 (2005) 1757

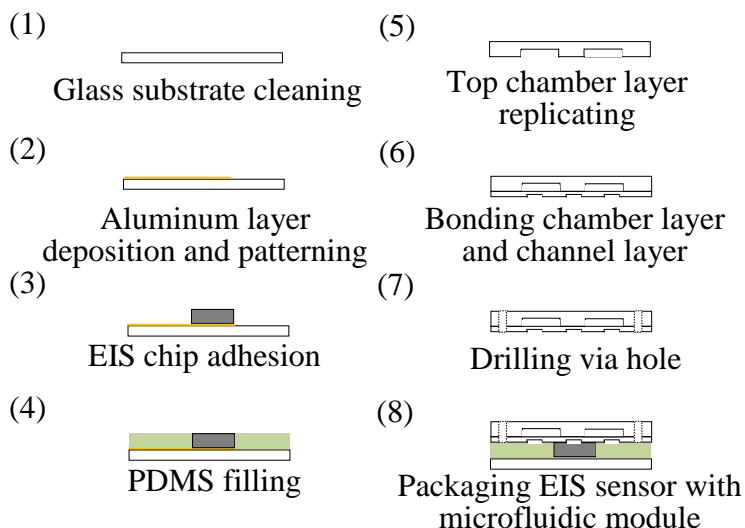
13. M. Castellarnau, N. Zine, J. Bausells, C. Madrid, A. Juarez, J. Samitier and A. Errachid, *Sens. Actuators B-Chem.*, 120 (2007) 615
14. L. Bousse, N.F. de Rooij and P. Bergveld, *IEEE Trans. Electron Devices*, 30 (1983) 1263
15. C.D. Fung, P.W. Cheung and W.H. Ko, *IEEE Trans. Electron Devices*, 33 (1986) 8
16. S.-B. Huang, M.-H. Wu and G.-B. Lee, *Sens. Actuators B-Chem.*, 147 (2010) 755
17. T.-M. Pan and C.-W. Lin, *J. Electrochem. Soc.*, 158 (2011) J100
18. M.J. Schoning, N. Nather, V. Auger, A. Poghossian and M. Koudelka-Hep, *Sens. Actuators B-Chem.*, 108 (2005) 986
19. J.-C. Chou, G.-C. Ye, D.-G. Wu and C.-C. Chen, *Solid-State Electron.*, 77 (2012) 87
20. K. Matsuura, Y. Asano, A. Yamada and K. Naruse, *Sensors*, 13 (2013) 2484
21. T. Masadome, S. Kugoh, M. Ishikawa, E. Kawano and S. Wakida, *Sens. Actuators B-Chem.*, 108 (2005) 888
22. T.-M. Pan, M.-D. Huang, C.-W. Lin and M.-H. Wu, *Sens. Actuators B-Chem.*, 144 (2010) 139
23. S. Sharma, A.R. Moniz, I. Triantis, K. Michelakis, J. Trzebinski, A. Azarbadegan, B. Field, C. Toumazou, I. Eames, A. Cass, *Microfluid. Nanofluid.*, 10 (2011) 1119

Supplemental Fig. S1



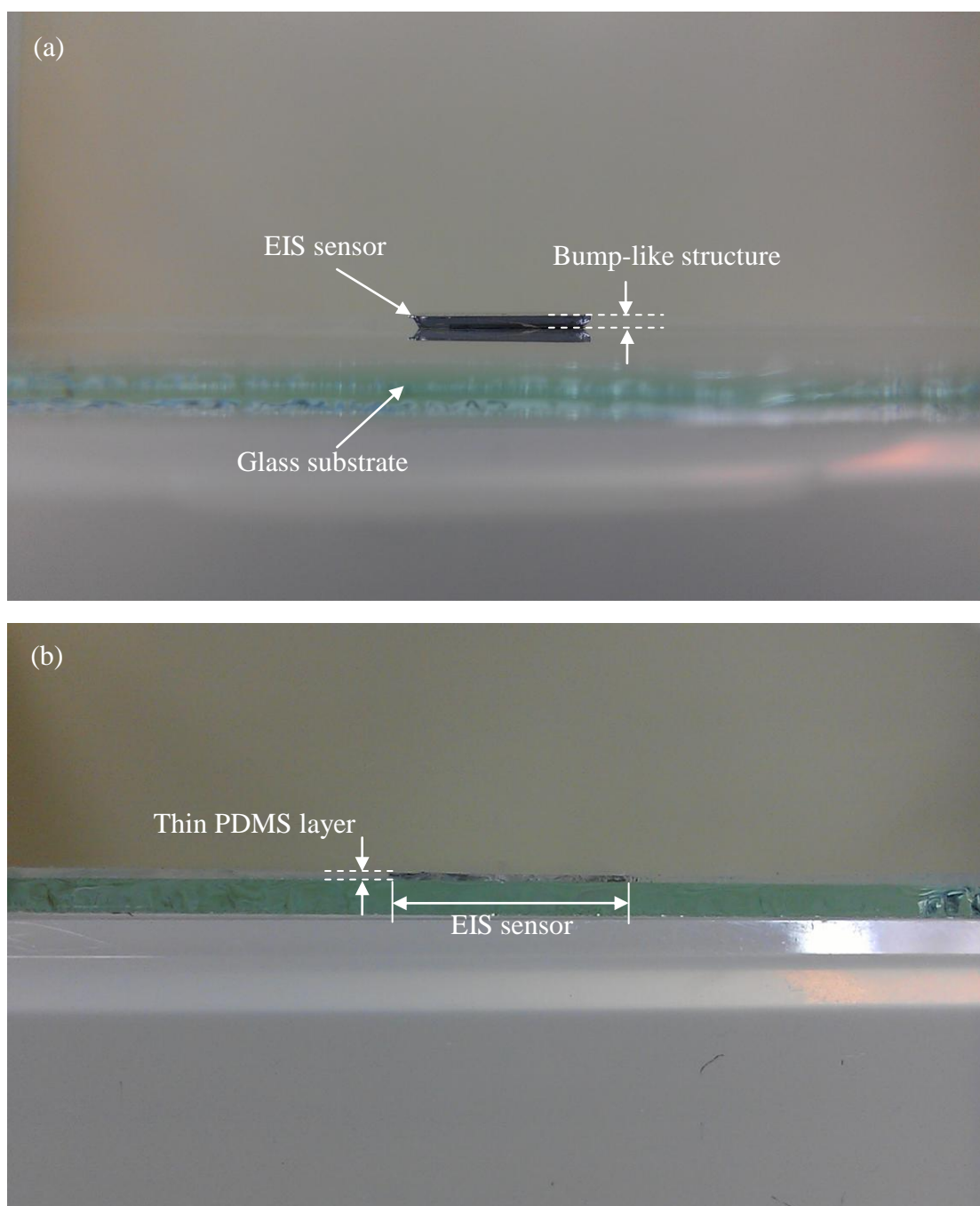
The working principle of the fluid transportation. (a) Schematic of the pneumatic micropump using time-delay peristaltic actuation. (b) Cross-sectional view of the actuation mechanism of the micropump. The micro-pump consists of three air chambers and an underlying microchannel. The chambers are filled with compressed air sequentially from the chamber closest to the compressed air inlet to the farthest one so that the PDMS membranes beneath the air chambers deflect sequentially in the downward direction and the fluid is transported accordingly.

## Supplemental Fig. S2



The top and bottom glass substrates with metal electrodes were fabricated by the standard lift-off process (figs. (1)-(2)). The difference is that the bottom substrate was coated with aluminium (300 nm), and the top one was coated with a silver (400 nm). The top substrate functions as a reference electrode, so the tip of the silver electrode was modified with  $\text{FeCl}_3$  to form Ag/AgCl layers. The modified process was optimized by dipping the silver thin film into a 0.05 M  $\text{FeCl}_3$  solution for 2 s. The EIS structure having a 20 nm, high-k,  $\text{Dy}_2\text{TiO}_5$ -sensing membrane was fabricated on 4-inch p-type Si (100) wafers with a rapid thermal annealing process at  $800^\circ\text{C}$  for 30 s in ambient  $\text{O}_2$ , which was based on our previous work [17]. Then, a layer of thin SU-8 photoresistors was used to define a circular sensing area that was 2 mm in diameter. After the EIS sensor was cut in a  $1 \times 1\text{ cm}^2$  area, the EIS sensor die was attached to the bottom glass substrate with the aluminium electrode using highly conductive silver glue (SYP-8888, AGPRO Technology Co., Ltd., Taiwan). The EIS sensor attached to the substrate forms a bump structure in the micro-channel that causes unstable flow or a dead volume around the bump structure. To address this issue, a thin PDMS layer was used to fill the bump structure, thus making the micro-channel flat (figs. (3)-(4)) (see detail in supplemental fig. S3). The microfluidic component layers were fabricated through the standard SU-8 (SU-8-50, MicroChem, USA) photolithography, micro-carving machining, and PDMS (Sylgard 184A and 184B, Sil-More Industrial Ltd., USA) replication processes (figs. (5)-(6)). After the hole was drilled, the PDMS layers were aligned and bonded to the bottom sensor substrate layer using an oxygen plasma treatment process (figs. (7)-(8)).

## Supplemental Fig. S3



A thin PDMS layer filled up the bump structure caused by silicon die and resulted in the same level of sensor surface and PDMS surface. Fig. S3 shows the bottom layer of the chip (a) before and (b) after the bump structure was filled up with the thin PDMS layer. Note that during fabrication process, another glass plate was placed on top of the sensor die such that the flat PDMS surface can be formed.